

# Dynamic Imaging and Tracer Kinetic Modeling for Emission Tomography Using Rotating Detectors

Chi-Hoi Lau, *Member, IEEE*, Dagan Feng,\* *Senior Member, IEEE*, Brian F. Hutton, *Senior Member, IEEE*, Daniel Pak-Kong Lun, *Member, IEEE*, and Wan-Chi Siu, *Senior Member, IEEE*,

**Abstract**—When performing dynamic studies using emission tomography the tracer distribution changes during acquisition of a single set of projections. This is particularly true for some positron emission tomography (PET) systems which, like single photon emission computed tomography (SPECT), acquire data over a limited angle at any time, with full projections obtained by rotation of the detectors. In this paper, an approach is proposed for processing data from these systems, applicable to either PET or SPECT.

A method of interpolation, based on overlapped parabolas, is used to obtain an estimate of the total counts in each pixel of the projections for each required frame-interval, which is the total time to acquire a single complete set of projections necessary for reconstruction. The resultant projections are reconstructed using traditional filtered backprojection (FBP) and tracer kinetic parameters are estimated using a method which relies on counts integrated over the frame-interval rather than instantaneous values. Simulated data were used to illustrate the technique's capabilities with noise levels typical of those encountered in either PET or SPECT. Dynamic datasets were constructed, based on kinetic parameters for fluoro-deoxy-glucose (FDG) and use of either a full ring detector or rotating detector acquisition. For the rotating detector, use of the interpolation scheme provided reconstructed dynamic images with reduced artefacts compared to unprocessed data or use of linear interpolation. Estimates for the metabolic rate of glucose had similar bias to those obtained from a full ring detector.

**Index Terms**—Coincidence detection, emission tomography, PET, SPECT, tracer kinetic modeling.

## I. INTRODUCTION

USING emission tomography it is possible to record the bio-distribution of radiopharmaceuticals within the body and the change of these distributions with time. Dynamic images can be reconstructed and information relating to function of the living human body can be directly visualized. Further-

more, parametric images depicting physiological parameters, such as the metabolic rate of glucose in tissue, can be derived from these dynamic images using modeling procedure [1]. A basic premise for extraction of quantitative parameters is that the time course of tracer in tissue can be reliably recorded. This can be achieved using stationary detectors as in the ring geometry most commonly available for positron emission tomography (PET) and similarly designed single photon emission computed tomography (SPECT) systems based on detector rings [2]–[4].

Recently, there has been interest in reducing the capital cost associated with PET studies with the introduction of systems which acquire data over a limited angle, with rotation over time [5], [6]. Also, coincidence studies have recently been performed using dual opposing detectors which are conventionally used for SPECT where the detectors rotate around the patient [7]. There is an increasing interest in deriving parametric images from these systems. In the case of SPECT there have been significant improvements in the quantitative accuracy of reconstruction as well as the development of multidetector cameras which permit efficient detection. As a consequence, acquisition of kinetic data with associated modeling is possible on these systems and has been demonstrated by a number of groups [8]–[11]. These systems have similar constraints to PET systems based on rotating detectors since, at any point in time, partial data are acquired, with the possibility of change in radiopharmaceutical distribution during the acquisition of the set of projections necessary for reconstruction. The resultant reconstructed images may contain artefacts which influence the accuracy of any subsequent parameter estimation [12]–[14]. The reduction of acquisition time is limited by the physical constraints of mechanical rotation, and by the low counts acquired by a system whose acquisition geometry limits detection efficiency.

The traditional modeling approach requires extraction of tracer time-activity curves which are fitted using an appropriate model to estimate the physiological parameters. An alternative approach is to estimate physiological parameters of the process directly from the projection data, reconstructing parametric images directly from projections, rather than a dynamic sequence of images. A general approach based on the weighted integration method was proposed for SPECT [15] and was previously applied to PET data [16]. Others have developed methods to recover the parameters of the time-activity curve in each pixel directly from the projection data [17], [18]. They have shown that they can accurately recover time-activity curves for a simple mono-exponential model. Extension to

Manuscript received May 20, 1996; revised November 19, 1998. This work was supported in part by the Australian Research Council (ARC) and the Hong Kong Polytechnic University under Grant 350/574. The Associate Editor responsible for coordinating the review of this paper and recommending its publication was C. Thompson. *Asterisk indicates corresponding author.*

C.-H. Lau, D. P.-K. Lun, and W.-C. Siu are with the Center of Multimedia Digital Signal Processing, Department of Electronic and Information, Engineering, The Hong Kong Polytechnic University, Hong Kong.

\*D. Feng is with the Center of Multimedia Digital Signal Processing, Department of Electronic and Information Engineering, The Hong Kong Polytechnic University, Hong Kong and the Biomedical and Multimedia Information Technology (BMIT) Group, Basser Department of Computer Science, The University of Sydney, N.S.W. 2006, Australia.

B. F. Hutton is with the Biomedical and Multimedia Information Technology (BMIT) Group, Basser Department of Computer Science, The University of Sydney, N.S.W. 2006, Australia, and the Department of Medical Physics, Westmead Hospital, Westmead, N.S.W. 2145, Australia.

Publisher Item Identifier S 0278-0062(98)09744-4.

more complex models may be feasible, although the solution is likely to be computationally demanding.

In this paper, we propose an approach for estimating the kinetic parameters from dynamic studies recorded by rotating detector systems, either single or multidetector SPECT or certain PET or coincidence detection systems. The method involves interpolation across projections so as to provide an improved estimate of the projections, closer to that obtained for a stationary detector system. This interpolation process is applicable either to estimation of parameters directly from projections or to solutions involving conventional reconstruction prior to kinetic modeling. In our case the interpolated projections are reconstructed using the conventional filtered backprojection (FBP) algorithm and the kinetic parameters are estimated using a modified weighted least squares cost function. The proposed method is based on several previously validated techniques which, in combination, provide a relatively simple and computationally efficient solution. To evaluate performance, we use the [ $^{18}\text{F}$ ] labeled fluoro-deoxy-glucose (FDG) model, as applied to tomographic studies of the brain, which has well documented kinetics and potential applications in both PET and coincidence imaging.

## II. THEORY FOR THE PROPOSED METHOD

### A. A Common Nomenclature for PET and SPECT Dynamics

To introduce the proposed approach it is useful to establish a nomenclature which is common to both PET and SPECT, specific to rotating detector systems as opposed to stationary systems. The usual mode of acquisition (typical of rotating camera SPECT systems) involves acquisition of projections at individual angular positions with rotation of the detectors between subsequent projection angles. It is useful to distinguish between the time taken to acquire a single projection and the time taken to acquire all projections which constitute a single rotation (or, more exactly, which would contribute to a single reconstruction). A dynamic sequence consists of multiple rotations. We define the following terms.

*Frame-interval* is the period of time for a complete rotation or acquisition of one complete set of projections (contributing to a single reconstruction). For example, a single head camera rotating over 360 degrees between times  $t_0$  and  $t_1$  would acquire all projections in the frame-interval  $[t_1 - t_0]$ . We use this term with reference to *frames* in the dynamic sequence as commonly used in nuclear medicine. For a stationary detector all projections are normally acquired simultaneously for the complete frame-interval. However, in a rotating detector system, each individual projection occupies a *projection-interval* which, for a single head camera equals the [frame-interval/number of angles]. The data for different projections will be acquired sequentially in each frame-interval. In the general case, neither the frame-interval nor the projection-interval are constant for sequential rotations. For any underlying tracer kinetics a time-activity curve can be postulated for a single pixel in the projection domain. At a given angle the acquisition over multiple rotations results in a set of measured samples of the underlying time-activity curve, each

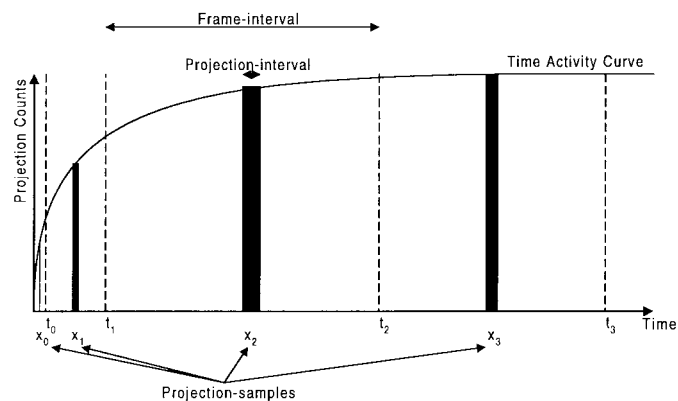


Fig. 1. Definition of frame-interval, projection-interval, and projection-sample. The solid curve simulates the actual tracer uptake curve. The solid black rectangles represent the projection samples which are taken as the count rates average over the projection-intervals centered at times  $X_i$ , where  $i = 0, 1, 2, 3$ . The times  $t_i$  where  $i = 0, 1, 2, 3$ , define the boundaries between adjacent frames.

sample occupying a projection-interval. We refer to these as projection-samples. For a stationary detector, where the projection-interval equals the frame-interval, the projection-sample is the total counts acquired for the frame-interval, though normally considered as a sample at the midpoint of the interval. In the case of the rotating detector the projection-sample is the total counts for the projection-interval. However, the total counts for the frame-interval for that projection pixel can only be determined by interpolation between projection-samples. We further define the selection of frame-intervals for the complete multirotation study as *frame-sampling* to remove any ambiguity with projection-sampling. Fig. 1 illustrates the definition of frame-interval, projection-interval and projection-sample.

### B. Basis of the Method

To accurately estimate kinetic parameters from a dynamic study normally necessitates acquisition of multiple short frames, particularly near the start of the study. These short frames tend to be noisy and may occupy considerable disk space. If instead longer acquisition times are used, then there is likely to be tracer redistribution during early frame-intervals which may result in artefacts. Our proposed approach is to use the minimum number of frames, minimizing disk space and processing time. An interpolation technique is used to minimize the influence of tracer redistribution on the results. Fundamental to the approach is the adoption of a strategy where parameters are estimated, based on total counts over the frame-interval [19]–[25], rather than using the normal assumption that measurements represent estimates of the instantaneous mid-interval values. Using the modified premise, a more accurate interpolation scheme can be defined in projection space [26] so that conventional reconstruction (e.g., using FBP) is feasible with reduced artefacts. The interpolation scheme adopted, unlike others, e.g., use of Simpson's rule [27], is not limited to acquisition with equal frame-intervals. Consideration of the optimal frame-sampling required for a specific model provides a solution with the minimum possible

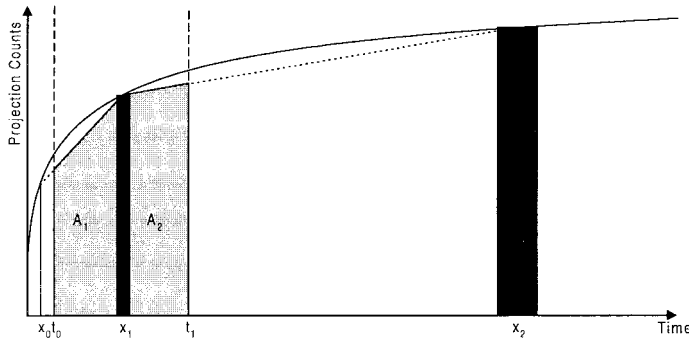


Fig. 2. Linear interpolation of projection data. For illustration purpose, this figure magnifies the early part of Fig. 1. For linear interpolation, we use straight lines (dotted lines) to interconnect the measured projection-samples at  $x_i$  and approximate the area under the solid curve for the relevant frame-interval (say,  $[t_0, t_1]$ ) by the area under the straight lines (i.e.,  $A_1 + A_2$ ).

number of frame-samples, with different duration for each frame [28]. The suggested approach is practical, requiring a small number of rotations of the detector system, each rotation of different duration. The detailed steps and techniques are outlined below.

### C. Estimation of Projections by Interpolation

The first step of the proposed approach is to estimate as accurately as possible, the total counts in each pixel of the projection data for each frame-interval so that more reliable dynamic images can be reconstructed. The simplest technique to achieve this is by linear interpolation [29] as illustrated in Fig. 2. For each pixel in the projection domain, we assume linear change of activity between projection-samples. We can then calculate the total counts within each frame-interval by summing the appropriate areas. We divide the total area by the corresponding frame-interval to obtain an average count-rate. It is recognized that this approach may be inaccurate for certain curve shapes (as illustrated). An alternative approach, based on the integration of overlapped parabolas, has therefore been developed [26]. The method is applicable to nonuniformly sampled measurements and can be efficiently computed.

The approach is illustrated in Fig. 3. We require to estimate the total counts between times  $t_i$  and  $t_{i+1}$ , with projection-samples for a given projection angle at times  $x_1, x_2, \dots, x_n$ , where  $n$  is the number of frame-intervals. For the projection-sample at  $x_j$  located in the frame-interval between  $t_i$  and  $t_{i+1}$ , a parabola is fitted to the projection samples at  $(x_{j-2}, x_{j-1}, x_j)$ . Integrating the function of this parabola from  $t_i$  to  $x_j$ , we obtain

$$S_i^{(1)} = \int_{t_i}^{x_j} y_i^{(1)}(t) dt$$

where  $y^{(1)}(t)$  is a second-order equation fitted to the projection samples  $(x_{j-2}, x_{j-1}, x_j)$ .

We can also fit another parabola via  $(x_{j-1}, x_j, x_{j+1})$  and obtain

$$S_{i+1}^{(2)} = \int_{t_i}^{x_j} y_{i+1}^{(2)}(t) dt$$

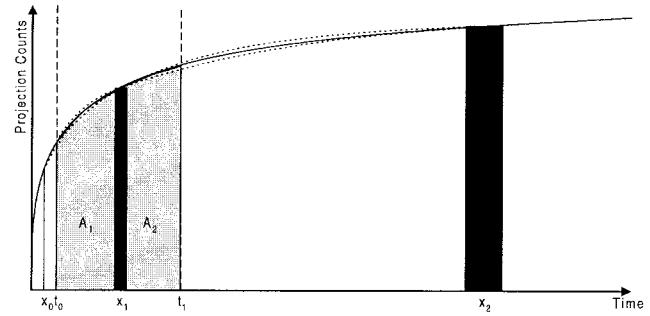


Fig. 3. Interpolation of projection data using the overlapped parabolas method. This figure magnifies the early part of Fig. 1. For overlapped parabolas, the area under the solid curve is estimated by averaging the area under two parabolas. For example,  $A_1$  is the average of the area under the two parabolas fitted with (origin,  $x_0, x_1$ ) and  $(x_0, x_1, x_2)$ , for the interval  $[x_1 - t_0]$  and  $A_2$  is the average of the area under the two parabolas fitted with  $(x_0, x_1, x_2)$  and  $(x_1, x_2, x_3)$ , for the interval  $[t_1 - x_1]$ . ( $x_3$  is not shown in this figure.) Then, the total area under the solid line within  $[t_0, t_1]$  is approximated by  $A_1 + A_2$ .

where  $y^{(2)}(t)$  is a second-order equation fitted to the projection samples  $(x_{j-1}, x_j, x_{j+1})$ .

Calculate the weighting coefficients,  $\alpha_i$ , as

$$\alpha_i = (t_{i+1} + t_{i+2} - t_i) / [2(t_{i+2} - t_{i-1})].$$

And overlapping the integral,  $S_i^{(1)}$  and  $S_i^{(2)}$ , we obtain

$$S_i = (1 - \alpha_i) S_i^{(1)} + \alpha_i S_{i+1}^{(2)}.$$

This provides an estimation on the total counts,  $S_i$ , within the segment from  $t_i$  to  $x_j$ . The total counts within the segment from  $x_j$  to  $t_{i+1}$  are similarly calculated using the appropriate projection-samples. The total counts between times  $t_i$  and  $t_{i+1}$  are calculated as the summation of the integrals of these two segments. These total counts are then divided by the corresponding frame-interval to obtain an average count-rate for the frame-interval  $[t_{i+1} - t_i]$ . The above interpolation process is applied to every pixel of the projections. The resultant projection data, which better approximate the projections for a stationary detector system, can then be used to reconstruct the dynamic images using FBP.

### D. Tracer Kinetic Modeling

After we obtain a dynamic set of reconstructed images, the next step is to perform physiological parameter estimation. Conventional modeling is based on the use of instantaneous curve values whose estimation may include significant error in the situation where the mid-interval estimates have been derived by taking the average over the frame-interval [19]. Instead we make use of a modified approach which is based on the area under the curve [20], [21]. This approach differs from the traditional technique in that a modified weighted least squares cost function or residual sum of squares (RSS) is defined.

Traditionally, RSS is defined as

$$\text{RSS} = \sum_{l=1}^L w_l \left[ y(t_l) - \bar{z}(t_l) \right]^2$$

where  $L$  is the number of samples,  $w_l$  is a weighting factor,  $y(t_l)$  is the *instantaneous* model-predicted count-rate at time  $t_l$ ,  $z(t_l)$  is the measured sample which is usually assumed to be the average count-rate for the frame-interval ( $\Delta t_l$ ) centered at  $t_l$ . The RSS denotes the residual differences between the measured tissue time activities,  $z(t_l)$ , and the estimated tissue time activities  $y(t_l)$ . The curve fitting procedure that we used in our simulation is the nonlinear least square (NLS) approach. When the NLS method is used, the model parameters are varied using the Levenberg–Marquardt algorithm until the RSS reaches its minimum. Once the optimized model parameters are obtained, the physiological parameter can be estimated.

The problem for such RSS is that, when the dynamics change rapidly,  $\Delta t_l$  must be sufficiently small, otherwise  $z(t_l)$  may not be a good approximation of the instantaneous measurement at  $t_l$ . In other words, we typically need a large number of frame-samples when the activity changes rapidly. To avoid this requirement, the RSS is modified to be

$$\text{RSS} = \sum_{l=1}^L w_l \left[ \overline{y(t_l)} - \overline{z(t_l)} \right]^2$$

where  $\overline{y(t_l)} = (1/\delta t_l) \int_{\Delta t_l} y(t) dt$  is the average model predicted count-rate over the frame-interval  $\Delta t_l$ . In this case approximation error will be eliminated. It has been shown [28] that, by using the above modified fitting algorithm, only four dynamic images are necessary to estimate the metabolic rate of glucose using the four-parameter FDG model. In this case  $\Delta t_l$  may be relatively large.

### III. SIMULATION METHOD

As indicated earlier we have chosen to validate the proposed method using the FDG model [1] which involves three compartments. The FDG concentration measured in blood plasma is normally used as the input function for the model. We generated the input function numerically using a model for the input function, a commonly adopted approach [30]–[32]. In our simulation, we used a plasma time-activity curve (PTAC) model which has been previously validated [33] and used in several previous simulation studies [34]–[36]. We assume that the time delay of the input function model is equal to zero. The mathematical expression of this simplified input function model  $Cp(t)$  is given as follows:

$$Cp(t) = (A_1 t - A_2 - A_3) \exp(\lambda_1 t) + A_2 \exp(\lambda_2 t) + A_3 \exp(\lambda_3 t)$$

where, as previously published [33]:

$$\begin{aligned} A_1 &= 851.1, & A_2 &= 21.88, & A_3 &= 20.81 \quad [\mu\text{Ci/ml}] \\ \lambda_1 &= -4.134, & \lambda_2 &= -0.1191, & \lambda_3 &= -0.0104 \quad [1/\text{min}]. \end{aligned}$$

The proposed method was tested using the phantom shown in Fig. 4 which contains three regions with different kinetics. Activities in the left ellipse, right ellipse and the circle were simulated to represent the kinetics which are typical of brain white matter (Region 1), grey matter (Region 2) and an intermediate value (Region 3). The resulting tracer time-activity curves are shown at the top right, middle right and

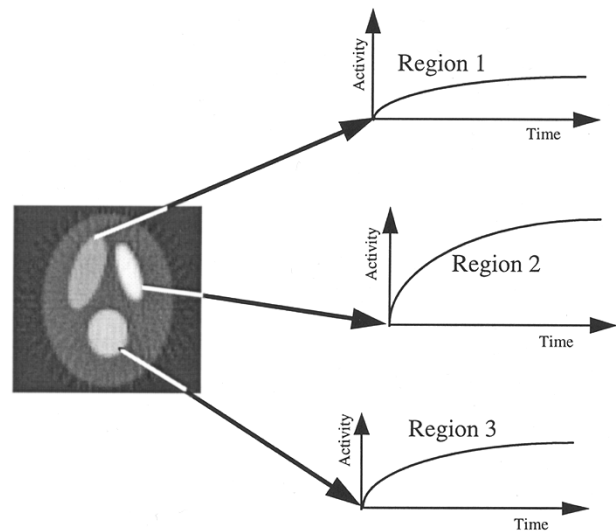


Fig. 4. Simulated phantom. The activity in the left ellipse (Region 1), right ellipse (Region 2), and the circle (Region 3) simulate the tracer kinetics of brain white matter, grey matter, and an intermediate value. The tracer time activity curves are shown at the top right, middle right, and bottom right, respectively.

TABLE I

	$k_1$	$k_2$	$k_3$	$k_4$	$K$
Right ellipse	0.1020	0.1300	0.0620	0.0068	0.0329
Left ellipse	0.0540	0.1090	0.0450	0.0058	0.0157
Circle	0.0780	0.1195	0.0535	0.0063	0.0241

bottom right respectively. The outer largest ellipse has constant activity. The transport rate constants,  $k_1 - k_4$ , for the three regions were obtained from [1] and are listed in Table I.

For simplicity,  $K = k_1 * k_3 / (k_2 + k_3)$ , which is proportional to the metabolic rate of glucose, is used as our final estimation result to compare the performance for different methods.

As indicated earlier, it has previously been demonstrated that the FDG kinetics can adequately be estimated by acquiring four frame-samples. According to [28], the four frames are of different duration and they are, in minutes, [0,2.7], [2.7,15.7], [15.7,77.1], [77.1,120]. For each of these frame-intervals 32 projections, each with 64 bins, were simulated.

Activity was simulated as the total counts detected over the complete frame-intervals as in conventional PET using a ring of detectors (Type A) and the counts corresponding to the projection-interval for a specific projection, assuming rotation of the detector (Type B). The simulation did not include attenuation, scatter or distance dependent detector response.

The projection data were scaled to count densities which might be expected for multidetector SPECT (with 0.02–0.05 k counts/s in the last frame-interval), coincidence imaging (with 0.1–0.2 k counts/s in the last frame-interval), and PET (with 1–2 k counts/s in the last frame-interval). Poisson noise was added to the projection data.

Four methods for analysis were compared. The data acquired with full ring geometry (Type A above) were reconstructed using FBP and kinetic modeling was performed on the reconstructed images using the modified RSS (Method 1). This method has fully recorded projection data for each

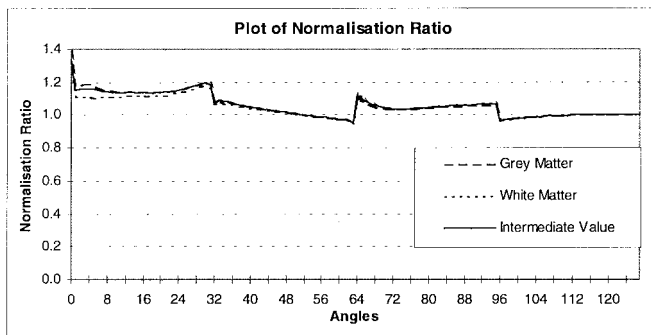


Fig. 5. The normalization ratio at different angles. The dashed line, dotted line, and solid line are the ratio for grey matter, white matter, and an intermediate value.

frame-interval. For the data acquired with a rotating detector (Type B above), the data were reconstructed and analyzed without interpolation (Method 2). For this Type B dataset, curve integrals on projections were also determined using interpolation (linear versus overlapped parabolas), prior to FBP reconstruction and modeling with the modified RSS approach (Methods 3 and 4). In the case of overlapped parabolas, projection data were normalized to account for systematic errors in the interpolation. To determine the appropriate normalization factors, true time-activity curves for a full ring detector system were simulated for the range of expected model parameters (typical of grey to white matter). The integrated counts for each frame-interval were compared to the integral estimated from the projection-samples which would be obtained from a rotating detector. The ratio of these integrals was used to normalize the projections. Fig. 5 shows the normalization ratio calculated at different angles. The dashed line, dotted line and the solid line represent ratios for grey matter, white matter and the intermediate value respectively. The systematic error was found to be reasonably independent of the underlying kinetic parameters and therefore normalization was based on the values obtained using the intermediate set of kinetic parameters (as per the third row of Table I).

$K$ , which is proportional to the metabolic rate for glucose, was estimated for the four different methods at different simulated count densities. For each count density, the simulations were carried out for one hundred independent trials to obtain average performances for each method. The percentage errors in  $K$  compared to the true parameters (bias) and the coefficient of variation (CV) of the estimated  $K$ 's were determined.

#### IV. RESULTS

Fig. 6 illustrates the first reconstructed frame of the simulated dynamic study for the four methods: (a) ring detectors, (b) rotating detectors with no interpolation, (c) linear interpolation, and (d) interpolation using overlapped parabolas. These images are noise-free to better illustrate the artefacts present when activity changes rapidly. Both linear interpolation and interpolation based on overlapped parabolas provide qualitatively improved reconstruction. The curves in Fig. 7 represent selected profiles through the same images as illustrated. For the left column of Fig. 7 the lower peak of the curves

represents the tracer activity in the left ellipse which has kinetic parameters simulating brain white matter. For the right column of Fig. 7 the highest peak represents the tracer activity of the right ellipse which simulates brain grey matter. For all six figures, the solid line represents data simulated for full ring detectors. The dotted line represents the data using a rotating detector: (a) and (b) with no interpolation, (c) and (d) using linear interpolation, and (e) and (f) using overlapped parabolas for interpolation. As can be seen, the use of overlapped parabolas for interpolation provides significant improvement compared to linear interpolation, resulting in close agreement with the result obtained for a ring detector system.

Based on the dynamic images reconstructed using the four different methods, the modified modeling technique was used for parameter estimation. The results for estimation of metabolic rate of glucose ( $K$ ) are illustrated in Fig. 8(a) and (b) where the bias and CV for  $K$  are displayed graphically. As would be expected, use of rotating detectors can introduce bias to parameter estimates. Although linear interpolation provides lower CV there is significant bias in the parameter estimates for all three regions in the phantom. The proposed interpolation method based on overlapped parabolas provides similarly low bias to the results obtained with a ring detector system although the CV was higher than that obtained using linear interpolation and in fact comparable to rotating detectors without interpolation.

#### V. DISCUSSION

There is increasing interest in analysis of kinetic data since the range of potentially useful tracers is expanding and suitable detection systems are becoming more affordable. However the accurate estimation of tracer kinetic parameters from low-cost tomographic systems, which typically do not have a full ring of detectors, is not straight-forward. Several groups have suggested approaches for determining kinetic parameters directly from projections to overcome the problems associated with rapidly changing activity. These approaches can provide unbiased parameter estimates for simple models but their general applicability has yet to be demonstrated. The approach suggested here is intrinsically simple, based mainly on the integrals of counts during the time course of a tracer rather than the instantaneous values. This provides the basis for the interpolation method for which the total counts in the frame interval is directly estimated, a modified parameter fitting algorithm and a frame-sampling scheme which would appear to be favorable for the situation where rotating detector systems are used. The proposed techniques are not computer intensive compared with methods where modeling is performed directly from projections and they therefore have appeal for general clinical application. Using the proposed method, artefact-free dynamic images, reflecting the bio-distribution of radiopharmaceuticals within the body, are available. Direct comparison of the proposed methods with alternative techniques will be the subject of future investigation and has not been included in this paper.

The simulation results presented here are intended to be illustrative rather than conclusive. FDG has been chosen,

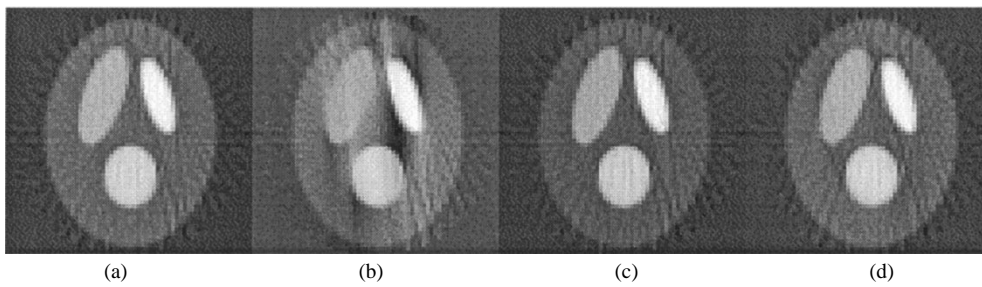


Fig. 6. Reconstructed images for the first frame-interval using the four different methods: (a) ring detectors, (b) rotating detectors without interpolation, (c) rotating detectors with linear interpolation, and (d) rotating detectors with interpolation using overlapped parabolas. These images are noise free to better illustrate the artefacts present when activity changes rapidly.

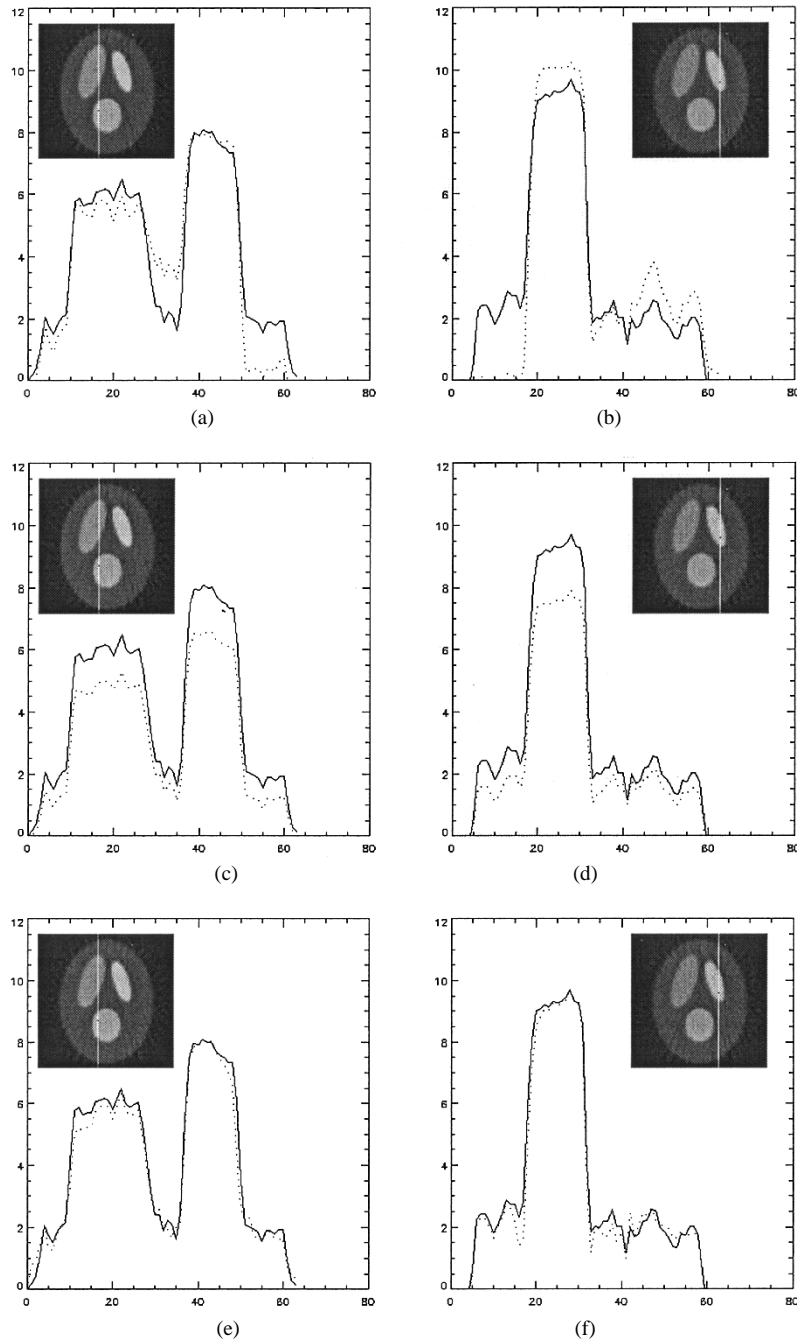


Fig. 7. Selected profiles through the images reconstructed using rotating detectors with different interpolation methods. The solid lines in all figures are from the data simulated for ring detectors. The dotted lines represent the profiles through the image reconstructed using rotating detectors with different methods: (a) and (b) without interpolation, (c) and (d) linear interpolation, and (e) and (f) interpolation based on overlapped parabolas. The lower and higher peaks of the curves on the left column simulate the tracer activity of Region 1 and Region 3, respectively. The highest peak on the right column simulates the tracer activity of the Region 2. These images correspond to noise-free data.

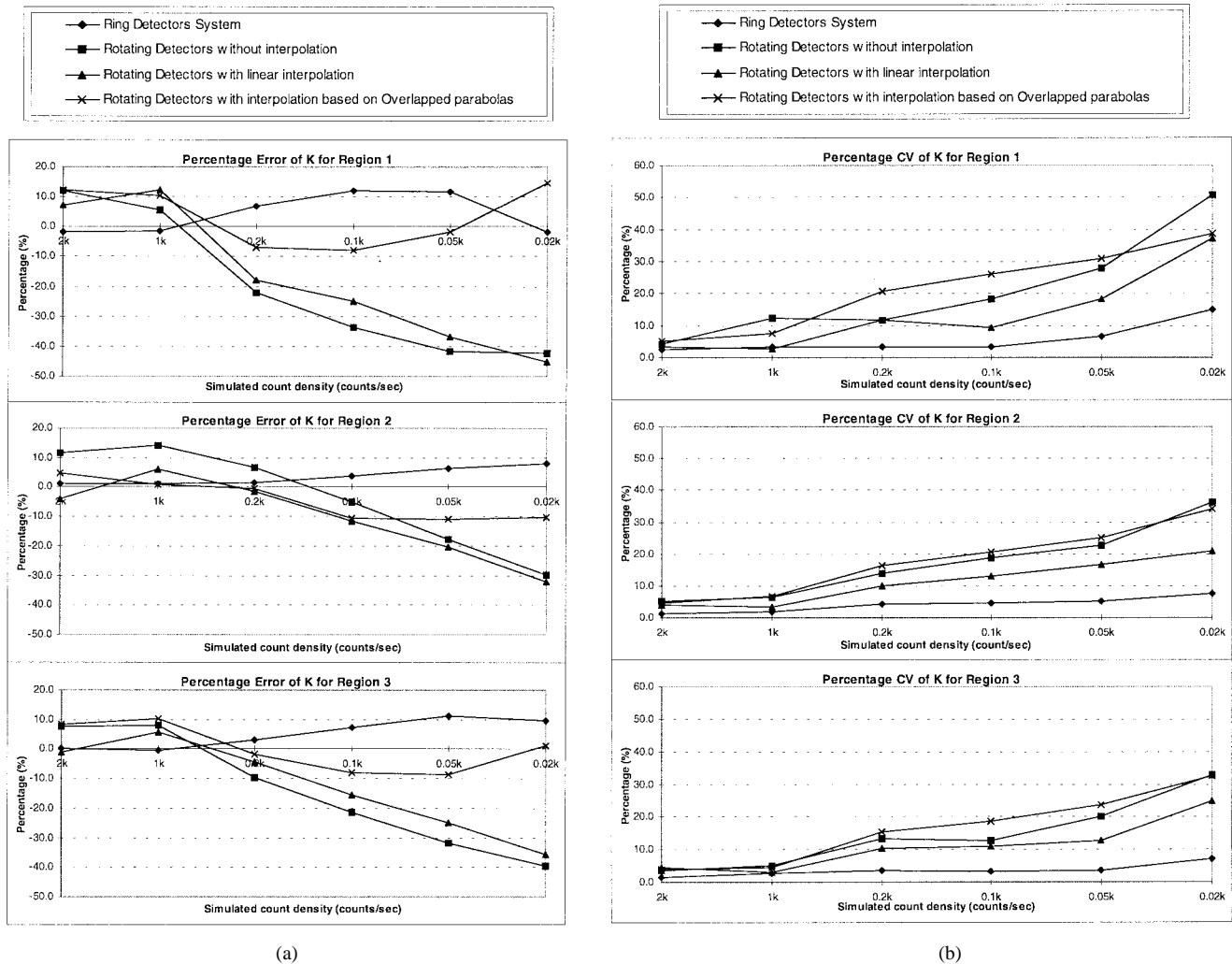


Fig. 8. (a) Percentage error of estimated K for the three regions and (b) CV of estimated K for the three regions.

given the interest in its application on low cost coincidence detection systems or rotating PET systems. The geometry of detection simulated is intended to illustrate the worst-case situation rather than to exactly simulate the detection geometry of a particular PET or SPECT system. Indeed the detection geometry more closely resembles a rotating SPECT system, for which the proposed methods have relevance. The paper does not address other physical constraints on the accuracy of measurement such as attenuation, scatter or, in the case of PET, random coincidences. Simplifications in the overall simulation were considered necessary to isolate the influences which were the primary concern in this paper (i.e., possibility of tracer movement in a single rotation). The input function can be accurately measured in patients based on counting of arterial blood samples (although less invasive methods are desirable). We did not examine the influence of input function shape on the results of this study, however we do not anticipate that the input function would be a dominant factor, as, in general, relatively small differences in input function shape occur between individuals for a given tracer.

The method of interpolation used in this paper has several appealing properties compared to some other interpolation schemes. First, it provides a valid integral rather than a

simple point value. As has been stated above, this has direct relevance to the proposed methods as it facilitates the use of optimized frame-sampling to reduce the number of detector rotations. The technique does not rely on having equally spaced frame-samples but is generally applicable for any sampling scheme. This paper does not address the question of how this technique compares with other nonlinear approaches to interpolation. It also does not explore the limits of the technique's application. However it is well demonstrated that, for the case of FDG, which is widely used in clinical practice, the technique provides results which are similar to those obtained for a stationary ring detector.

One problem with the interpolation method is the difficulty in handling points near the start of the study. The reason for this is that two of the three points used for fitting the parabola are very close together (the first point at time zero). As a result the best-fit parabola can deviate significantly from the true curve. Our results (Fig. 5) demonstrate that the problem is small except for a small number of projections. There are alternative approaches to solve this problem (e.g., constraint in the turning value of the parabola could be applied). However in this paper we have chosen to adopt a normalization method which applies a correction based on the range of errors which

could be anticipated for the family of possible kinetic curves. This method provided a practical solution with good results. Further work would be necessary to compare alternative strategies.

The simulation uses a frame-sampling scheme which particularly favors relatively low efficiency detection such as in SPECT. It has been demonstrated that the choice of four frame-samples is sufficient for accurate determination of the kinetic parameters for FDG. The use of four frame-samples has appeal since this minimizes the data storage requirements as well as minimizing the time required for reconstruction.

Parameter estimates for data acquired using a rotating detector were very close to those obtained using a stationary ring detector. However the coefficient of variation for parameter estimates was larger. It is clear that interpolation, based on noisy projection-samples, introduces an uncertainty in the derived frame-sample counts used to determine the parameter estimates. This resulted in an increased CV, particularly in the case of low count density.

## VI. CONCLUSIONS

In this paper, we proposed a novel approach for reconstruction of dynamic images and determination of tracer kinetic parameters using data acquired from a rotating detector system. The method involves the use of an interpolation method which provides an improved estimate of the total counts within each frame-interval, together with application of an integral-based model-fitting algorithm. The reliability of the proposed method has been tested by computer simulations over a range of count densities. The results demonstrate that the proposed approach provides artefact-free images and parameter estimates comparable to those obtained with a ring detector system, as is typical of conventional PET. The technique can potentially be applied to data acquired using systems such as single or multidetector SPECT, coincidence detection or low-cost PET systems which involve detector rotation rather than a stationary ring of detectors. The techniques therefore have widespread clinical appeal.

## REFERENCES

- [1] S. C. Huang, M. E. Phelps, E. J. Hoffman, K. Sideris, C. J. Selin, and D. E. Kuhl, "Noninvasive determination of local cerebral metabolic rate of glucose in man," *Amer. J. Physiol.*, vol. 238, pp. E69–E82, 1980.
- [2] E. M. Stokely, E. Sveinsdottir, N. A. Lassen, and P. Rommer, "A single-photon dynamic computer-assisted tomograph (DCAT) for imaging brain function in multiple cross-sections," *J. Comput. Assist. Tomogr.*, vol. 41, pp. 230–240, 1980.
- [3] I. Kanno, K. Uemura, Y. Miura, S. Miura, Y. Hirose, K. Koga, and H. Hattori, "The Headtome: A hybrid emission tomograph for brain. Design concepts and preliminary results," in *Proc. Medical Radionuclide Imaging 1980*, vol. 1, pp. 153–164.
- [4] B. L. Holman, P. A. Carvalho, R. E. Zimmerman, K. A. Johnson, S. S. Tume, A. P. Smith, and S. Genna, "Brain perfusion SPECT using an annular single crystal camera: Initial clinical experience," *J. Nucl. Med.*, vol. 31, pp. 1456–1461, 1990.
- [5] D. W. Townsend, M. Wensveen, L. G. Byars, A. Geissbuhler, H. J. Tochon-Danguy, A. Christian, M. Defrise, D. L. Bailey, S. Grootenok, and A. Donath, "A rotating PET scanner using BGO block detectors: Design, performance and applications," *J. Nucl. Med.*, vol. 34, pp. 1367–1376, 1993.
- [6] J. S. Karp, G. Muehllehner, D. A. Mankoff, C. E. Ordonez, J. M. Ollinger, M. E. Daube-Witherspoon, A. T. Haigh, and D. J. Beerbohm, "Continuous-slice PENN-PET: A positron tomograph with volume imaging capability," *J. Nucl. Med.*, vol. 31, pp. 617–627, 1990.
- [7] P. Nellesmann, H. Hines, W. Braymer, G. Muehllehner, and M. Geagan, "Performance characteristics of a dual head SPECT scanner with PET capability," in *IEEE Nuclear Science Symposium and Medical Imaging Conf. Rec.*, vol. 3, pp. 1751–1755, 1995.
- [8] A. M. Smith, G. T. Gullberg, P. E. Christian, and F. L. Datz, "Kinetic modeling of teboroxime using dynamic SPECT imaging of a canine model," *J. Nucl. Med.*, vol. 35, pp. 484–495, 1994.
- [9] H. Iida, H. Ito, M. Munaka, P. M. Bloomfield, S. Higano, M. Murakami, A. Inugami, S. Eberl, Y. Aizawa, I. Kanno, and K. Uemura, "A clinical method to quantitative CBF using a rotating gamma camera and I-123 amphetamine (IMP) with one blood sampling," *Eur. J. Nucl. Med.*, vol. 21, pp. 1072–1084, 1994.
- [10] H. Iida, H. Ito, M. Nakazawa, J. Hatazawa, H. Nishimura, Y. Onishi, and K. Uemura, "Quantitative mapping of regional cerebral blood flow using [123I] *N*-isopropyl-*p*-iodoamphetamine (IMP) and single photon emission tomography," *J. Nucl. Med.*, vol. 35, pp. 2019–2030, 1994.
- [11] M. Ichise, J. R. Ballinger, H. Golan, D. Vines, A. Luong, S. Tsai, and H. F. Kung, "Noninvasive quantification of dopamine D2 receptors with iodine-123-IBF SPECT," *J. Nucl. Med.*, vol. 37, pp. 513–520, 1996.
- [12] K. Tan, B. F. Hutton, and D. Feng, "Assessment of errors due to changing activity during kinetic SPECT acquisition," in *Proc. 17th Annu. Int. Conf. IEEE Engineering in Medicine and Biology Society*, ISBN 0-7803-2478-1 available: CDROM, Sept. 1995.
- [13] J. M. Links, T. L. Frank, and L. C. Becker, "Effect of differential tracer washout during SPECT acquisition," *J. Nucl. Med.*, vol. 32, pp. 2253–2257, 1991.
- [14] J. E. Juni, "SPECT of rapidly cleared tracers: Imaging a Cheshire cat," *J. Nucl. Med.*, vol. 33, pp. 1206–1208, 1992.
- [15] K. Tan, B. F. Hutton, and D. Feng, "A new approach for parameter estimation in SPECT dynamics using a rotating camera," *Eur. J. Nucl. Med.*, vol. 21 [Suppl], no. S29, 1994.
- [16] R. E. Carson, S. C. Huang, and M. V. Green, "Weighted integration method for local cerebral blood flow measurements with positron emission tomography," *J. Cereb. Blood Flow Metab.*, vol. 6, pp. 245–258, 1986.
- [17] M. A. Limber, M. N. Limber, A. Celler, J. S. Barney, and J. M. Borwein, "Direct reconstruction of functional parameters for dynamic SPECT," *IEEE Trans. Nucl. Sci.*, vol. 42, pp. 1249–1255, 1995.
- [18] G. L. Zeng, G. T. Gullberg, and R. H. Huesman, "Using linear time-invariant system theory to estimate kinetic parameters directly from projection measurements," *IEEE Trans. Nucl. Sci.*, vol. 42, pp. 2339–2346, 1995.
- [19] K. Chen, S. C. Huang, and D. Feng, "New estimation methods that directly use the time accumulated counts in the input function in quantitative dynamic PET studies," *Phys. Med. Biol.*, vol. 39, pp. 2073–2090, 1994.
- [20] R. Hawkins, M. E. Phelps, and S. C. Huang, "Effects of temporal sampling, glucose metabolic rates, and disruptions of the blood-brain barrier on the FDG model with and without a vascular compartments: Studies in human brain tumors with PET," *J. Cereb. Blood Flow Metab.*, vol. 6, pp. 170–183, 1986.
- [21] B. Mazoyer, R. H. Huesman, T. F. Budinger, B. L. Knittel, "Dynamic PET Data Analysis," *J. Comp. Assist. Tomogr.*, vol. 10, pp. 645–653, 1986.
- [22] P. C. Chiao, W. L. Rogers, N. H. Clinthorne, J. A. Fessler, and A. O. Hero, "Model-based estimation for dynamic cardiac studies using ECT," *IEEE Trans. Med. Imag.*, vol. 13, pp. 217–227, 1994.
- [23] I. Kanno, A. A. Lammersma, J. D. Heather, J. M. Gibbs, C. G. Rhodes, J. C. Clark, and T. Jones, "Measurement of cerebral blood flow using bolus inhalation of C15O2 and positron emission tomography: Description of the method and its comparison with the C15O2 continuous inhalation method," *J. Cereb. Blood Flow and Metab.*, vol. 4, pp. 224–234, 1984.
- [24] E. Tsui and T. F. Budinger, "Transverse section imaging of mean clearance time," *Phys. Med. Biol.*, vol. 23, pp. 644–653, 1978.
- [25] P. Herscovitch, J. Markham, and M. E. Raichle, "Brain blood flow measured with intravenous O-15 water I: Theory and error analysis," *J. Nucl. Med.*, vol. 24, pp. 782–789, 1983.
- [26] Z. Wang and D. Feng, "Continuous-time system modeling using the weighted-parabola-overlapping numerical integration method," *Int. J. Syst. Sci.*, vol. 23, pp. 1361–1369, 1992.
- [27] P. J. Davis and P. Rabinowitz, *Methods of Numerical Integration*. New York: Academic, 1975.
- [28] X. Li, D. Feng, and K. Chen, "Optimal image sampling schedule: A new effective way to reduce dynamic image storage space and functional image processing time," *IEEE Trans. Med. Imag.*, vol. 15, pp. 710–719, 1996.

- [29] B. E. Oppenheim and J. D. Krepschaw, "Dynamic hepatobiliary SPECT: A method for tomography of a changing radioactivity distribution," *J. Nucl. Med.*, vol. 29, pp. 98–102, 1988.
- [30] A. Kato, D. Menon, M. Diksic, and L. Yamamoto, "Influence of the input function on the calculation of the local cerebral metabolic rate of glucose in the deoxyglucose method," *J. Cere. Blood Flow Metab.*, vol. 4, pp. 41–46, 1984.
- [31] S. Takikawa, V. Dawan, P. Spetsieris, W. Robeson, T. Chaly, R. Dahl, D. Margouleff, and D. Eidelberg, "Noninvasive quantitative fluorodeoxyglucose PET studies with an estimated input function derived from a population-based arterial blood curve," *Radiol.*, vol. 188, pp. 131–136, 1993.
- [32] R. L. Philips, C.Y. Chen, D. F. Wong, and E. D. London, "An improved method to calculate cerebral metabolic rates of glucose using PET," *J. Nucl. Med.*, vol. 36, pp. 668–679, 1995.
- [33] D. Feng, S. C. Huang, and X. Wang, "Models for computer simulation studies of input functions for tracer kinetic modeling with positron emission tomography," *Int. J. Biomed. Comput.*, vol. 32, pp. 95–110, 1993.
- [34] D. Feng, X. Wang, and H. Yan, "A computer simulation study on the effects of input function sampling schedules in tracer kinetic modeling with positron emission tomography (PET)," *Comput. Meth. Programs Biomed.*, vol. 45, pp. 175–186, 1994.
- [35] D. Feng and X. Wang, "A method for biomedical system modeling and physiological parameter estimation using indirectly measured input functions," *Int. J. Sys. Sci.*, vol. 26, pp. 723–739, 1995.
- [36] D. Feng, X. Li, and S. C. Huang, "A new double modeling approach for dynamic cardiac PET studies using noise and spillover contaminated LV measurements," *IEEE Trans. Biomed. Eng.*, vol. 43, pp. 319–327, 1996.